optica

Laser writing of individual nitrogen-vacancy defects in diamond with near-unity yield: supplementary material

YU-CHEN CHEN[1†], BENJAMIN GRIFFITHS[1,2], LAIYI WENG[1], SHANNON NICLEY[1], SHAZEAA N. ISHMAEL[1], YASHNA LEKHAI[3], SAM JOHNSON[1], COLIN J. STEPHEN[3], BEN L. GREEN[3], GAVIN W. MORLEY[3], MARK E. NEWTON[3], MARTIN J. BOOTH[2], PATRICK S. SALTER[2], AND JASON M. SMITH[1*]

[1]Department of Materials, University of Oxford, Parks Road, Oxford OX1 3PH, UK
[2]Department of Engineering Science, University of Oxford, Parks Road, Oxford OX1 3PJ, UK
[3]Department of Physics, University of Warwick, Coventry CV4 7AL, UK
† Current address – 3 Physikalisches Institut, Universität Stuttgart, 70550 Stuttgart, Germany
* jason.smith@materials.ox.ac.uk

Published 10 May 2019

This document provides supplementary information to "Laser writing of individual nitrogen-vacancy defects in diamond with near-unity yield," https://doi.org/10.1364/OPTICA.6.000662.

Hanbury Brown and Twiss data

The datasets shown in Figure S1 were fitted with the following analytic function for the photon autocorrelation of a three-level system, which is established using a system of coupled rate equations

$$g^{(2)}(\tau) = 1 - ce^{-|\tau|/\tau_2} + (c-1)e^{-|\tau|/\tau_3}$$

where c, τ_3 and τ_2 are constants related to the internal dynamics of the NV center. Figure S2 shows the same data after it has been corrected for background fluorescence from the diamond, as described in the experimental methods section.

Fluorescence polarization data

Polarization measurements of the NV fluorescence are taken by placing a linear polarizing filter (Thorlabs LPVIS100) before a single photon detecting diode. The fluorescence intensity is measured as a function of polarizer angle, θ, using a motorized rotation mount (Thorlabs K10CR1/M). The measurements for each center in the array are presented in figure 4. The data are fitted according to a Malus-law function:

$$I(\theta) = I_0 + \Delta I cos^2(\theta + \varphi)$$

where I_0 is the minimal intensity, ($I_0 + \Delta I$) is the peak intensity and φ represents orientation of the of emission dipole projection on the plane of the microscope.

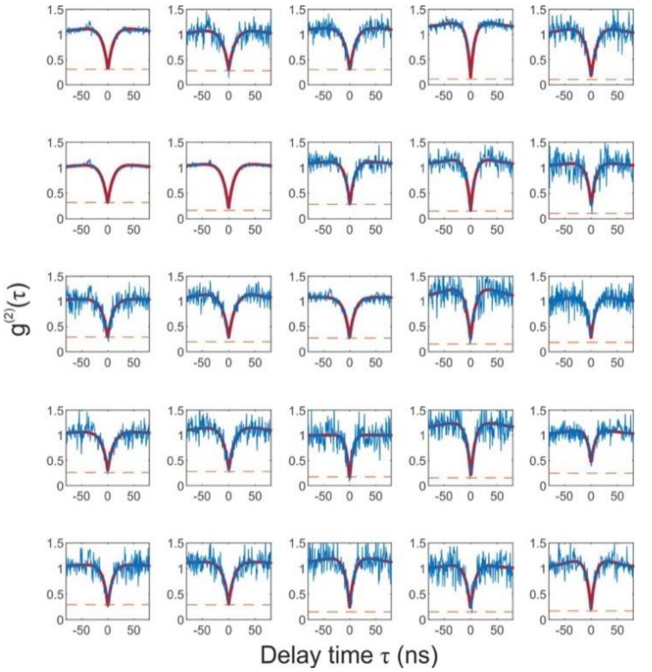

Figure S1: Uncorrected Hanbury-Brown and Twiss datasets for the array in Fig 1D. The dashed lines indicate the background levels calculated using the method described in the experimental methods section.

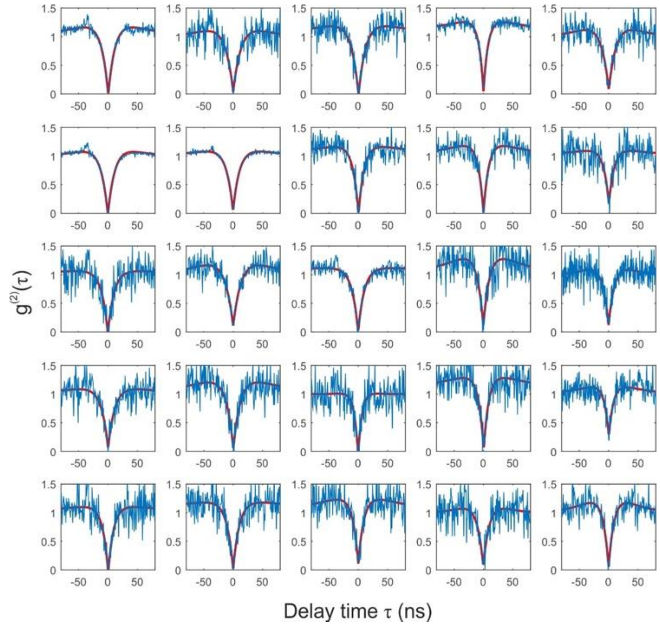

Figure S2: Autocorrelation data for the array in Fig 1D corrected for the effects of background signal from the bulk crystal.

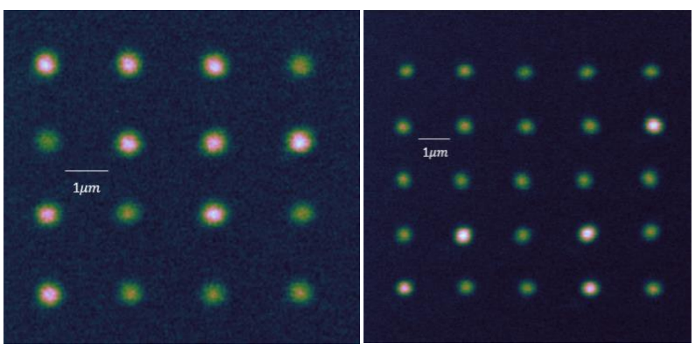

Figure S3: A 4 x 4 array and a 5 x 5 array of NV's created by laser processing. The array on the left was written by terminating processing upon measurement of a count rate in the range 11-15 kcounts/s, while the array on the right corresponds to processes terminated when a fluorescence count rate in the range 8-11 kcounts/s was measured. Single NV yields are 94% and 96% respectively.

Data from additional laser-written arrays

Figure S3 shows an additional 4 x 4 and 5 x 5 array of NV centers created by laser processing, with single NV yields of 94% and 96% respectively. These are the arrays created for the orientation-selective experiments, statistical data for which are presented in Figure 7E.

The 4x4 array was written by terminating processing upon measurement of a count rate in the range 11-15 kcounts/s. 15 of the 16 sites are single NV centers with 14 of these oriented out-of-plane. The 16th site contains two in-plane NV centers (Figure S4).

The 5x5 array corresponds to processes terminated when a fluorescence count rate in the range 8-11 kcounts/s was measured, aimed at creating a majority of in-plane oriented NV centers. 20 of the 25 sites contain single in-plane NV centers, whilst 4 sites contain single out-of-plane centers and 1 site contains two in-plane centers.

Fluorescence polarization data for these two additional arrays are shown in Figure S4.

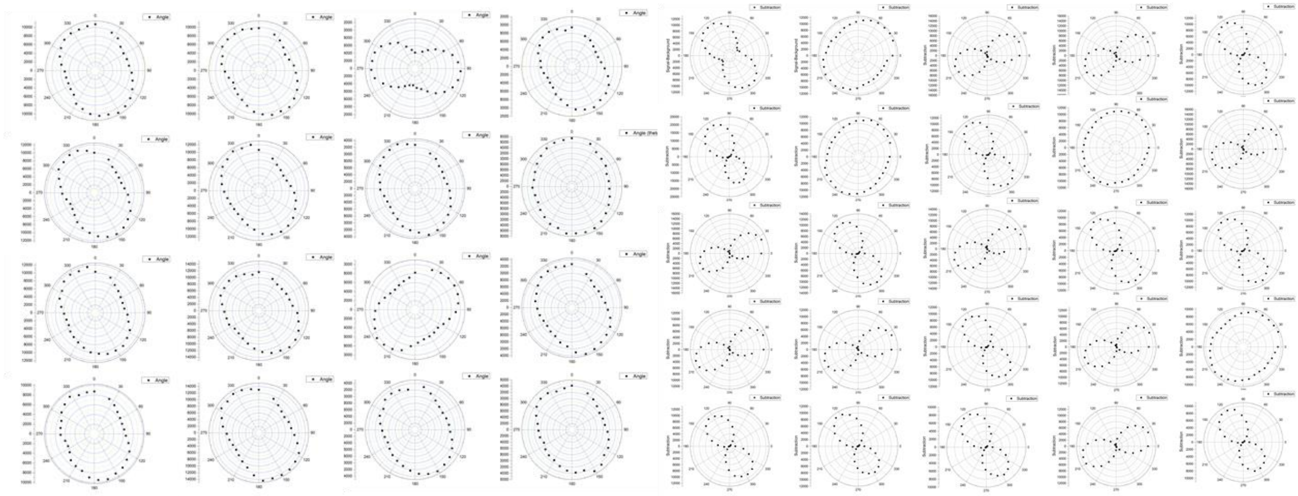

Figure S4: Fluorescence polarization plots of the arrays shown in Figure S3. The left hand array resulted from processing terminated when a fluorescence count rate of 11-15 kcts/s was observed and shows predominantly out-of-plane orientations; the right hand array resulted from processing when a count rate of 8 -11 kcts/s was observed and shows predominantly in-plane orientations.

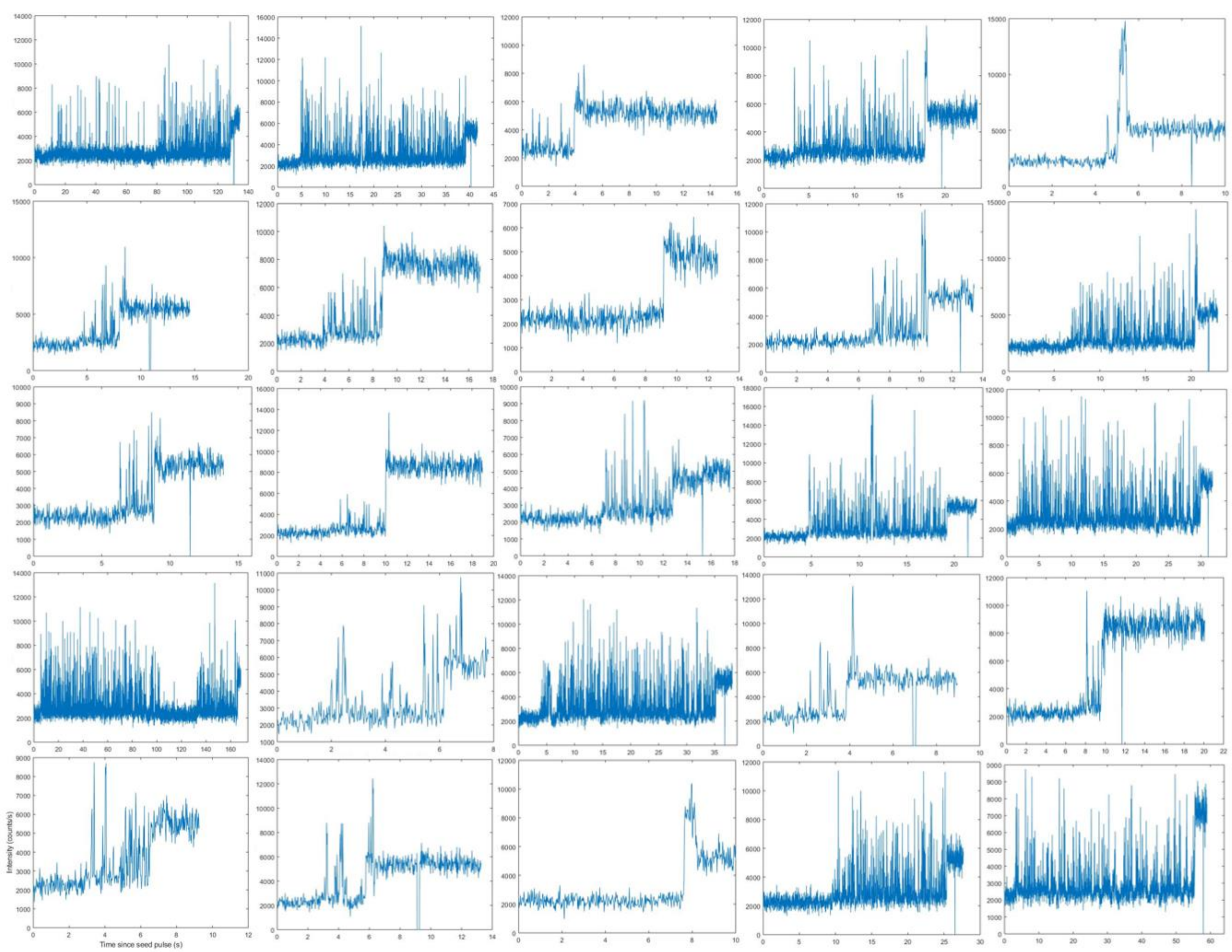

Figure S5: Fluorescence monitor traces for the array of NV centers displayed in Figure 3. Processing was stopped when a stable higher level of fluorescence was observed.

Fluorescence feedback time traces

Fluorescence time traces shown in Figure S5 display the collected fluorescence during the processing of the 25 sites in Figure 3. Fluorescence intermittently spiked during processing and then settled at the higher level when a stable NV was formed. Processing was then stopped when stable fluorescence was observed.

Room temperature spectrum

Figure S6 displays a room temperature spectrum of one of the NV centers from the array in figure 3, filtered only by a 532 nm notch filter and a 550 nm dichroic. After subtraction of the background signal, a clear spectrum of the NV^- defect is observed, with no evidence of emission from the NV^0 charge state.

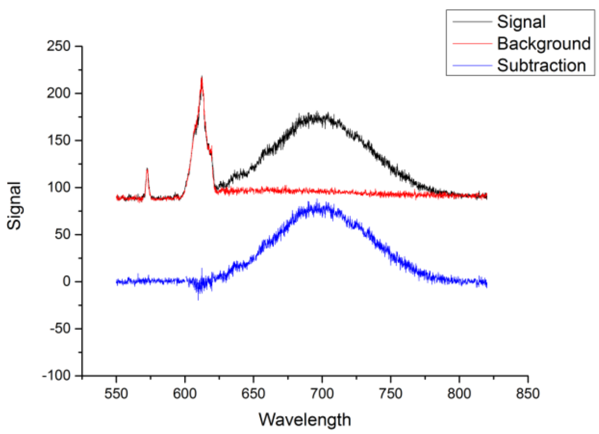

Figure S6: Full room temperature fluorescence spectrum of an NV center from the array in Figure 3. The black line shows the spectrum measured when focused on the center, the red line shows the background spectrum. The blue line is a subtraction of the two. The peaks at 573 nm and 600 nm are the first order and second order Raman lines from the diamond. The broad peak from 620 nm to 760 nm is the NV- spectrum with a small zero phonon line peak at 637 nm.

The research materials supporting this publication can be accessed by contacting jason.smith@materials.ox.ac.uk